Eur. Phys. J. Appl. Phys. **31**, 31–36 (2005)
DOI: 10.1051/epjap:2005040

THE EUROPEAN PHYSICAL JOURNAL APPLIED PHYSICS

Diode-pumped passively Q-switched intracavity-frequency-doubling Nd:$GdVO_4$/KTP green laser with Cr^{4+}:YAG saturable absorber

G. Li[a], S. Zhao, K. Yang, and D. Li

School of Information Science and Engineering, Shandong University, Jinan 250100, P.R. China

Received: 21 December 2004 / Received in final form: 29 January 2005 / Accepted: 4 February 2005
Published online: 21 June 2005 –

Abstract. The intracavity photon density is assumed to be Gaussian spatial distributions and the nonlinear loss that is due to second-harmonic generation (SHG) to the photon-density equation is given under Gaussian spatial distributions in the rate equations for a diode-pumped passively Q-switched intracavity-frequency-doubling Nd:$GdVO_4$/KTP laser with Cr^{4+}:YAG saturable absorber. These space-dependent rate equations are solved numerically. The dependences of pulse width, pulse repetition rate, single-pulse energy and peak power on incident pump power are obtained for the generated-green-laser pulses. In the experiment, a diode-pumped passively Q-switched intracavity-frequency-doubling Nd:$GdVO_4$/KTP laser with Cr^{4+}:YAG saturable absorber is realized and the experimental results are consistent with the numerical solutions.

PACS. 42.55.Ah General laser theory – 42.55.Xi Diode-pumped lasers – 42.60.Gd Q-switching

1 Introduction

Laser-diode-pumped all-solid-state passively-Q-switched lasers [1,2], due to the advantages of miniature, simplicity, compactness, high efficiency and low cost, have wide applications in the fields of remote sensing, ranging, medicine, etc. It is easy to obtain high nonlinear conversion efficiency by placing the nonlinear crystal into the laser resonator due to its high fundamental wave power density [3,4].

Nd:YVO_4 and Nd:YAG are very efficient laser materials for diode pumping. As a new host material for Nd^{3+} ion, the $GdVO_4$ crystal has been developed recently by Zagumennyi et al. [5], and Nd:$GdVO_4$ has been experimentally confirmed to be a promising laser medium for diode pumping [6]. Although $GdVO_4$ and YVO_4 crystals belong to the group of oxide compounds crystallizing in a Zircon structure with a tetragonal space group [7], it has been shown that Nd:$GdVO_4$ crystals have essential advantages in comparison with Nd:YVO_4 and Nd:YAG.Compared with Nd:YAG crystals, Nd:$GdVO_4$ has a 7-times higher absorption cross section at 808 nm ($\sigma_a = 5.2 \times 10^{-19}\,\mathrm{cm}^2, E\|c$) and a 3-times larger emission cross section at 1.06 μm ($\sigma_e = 7.6 \times 10^{-19}\ \mathrm{cm}^2$, $E\|c$) [6]. Compared with Nd:YVO_4 crystals, Nd:$GdVO_4$ has a much larger thermal conductivity along the $\langle 110\rangle$ direction at 300 K (about 11.7 W $\mathrm{m}^{-1}\,\mathrm{K}^{-1}$), which is more than a factor of two higher than that of Nd:YVO_4 and is even higher than that of Nd:YAG crystals [8]. A further advantage of Nd:$GdVO_4$ is the broad absorption with 3.2 nm FWHM of the pump transition at 808.4 nm. This results in a good spectral overlap between the diode-laser emission and the absorption of Nd:$GdVO_4$ without the need of diode-laser temperature control [6]. Such unique spectroscopic and thermal properties make Nd:$GdVO_4$ crystal a promising substitute for Nd:YAG and Nd:YVO_4 in diode-pumped compact solid-state lasers. During the past few years, diode-pumped Q-switched Nd:$GdVO_4$ lasers have been studied [9–11]. Actively Q-switched intracavity-frequency-doubling Nd:$GdVO_4$ lasers and passively Q-switched intracavity-frequency-doubling Nd:$GdVO_4$/Cr^{4+}:YAG laser have been also experimentally studied without any theoretical analysis [12–14].

Rate equations are efficient tools for analyzing the performance of a Q-switched laser. An accurate and general theoretical model of a LD-pumped passively Q-switched intracavity-frequency-doubling laser has been studied [15], in which the intracavity photon density is assumed to be Gaussian spatial distributions and the longitudinal variation of the intracavity photon density is also considered. But in reference [15], the nonlinear loss that is due to second-harmonic generation (SHG) [2] to the photon-density equation is given under an uniform plane-wave approximation. To obtain a more accurate theoretical analysis of the pulses from a LD-pumped passively Q-switched intracavity-frequency-doubling laser, the nonlinear loss due to SHG should be given under Gaussian spatial distributions.

[a] e-mail: guiqiu_li@hotmail.com

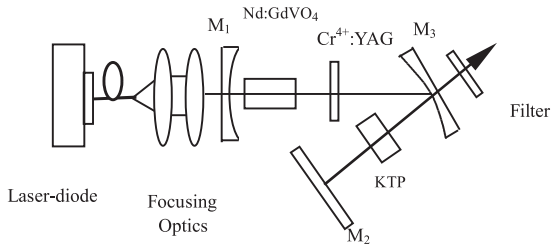

Fig. 1. Schematic of the experimental setup.

In this paper, we introduce the rate equations of a diode-pumped passively Q-switched intracavity-frequency-doubling Nd:$GdVO_4$/KTP laser with Cr^{4+}:YAG saturable absorber, in which the intracavity photon density is assumed to be Gaussian spatial distributions and the nonlinear loss due to SHG is also given under Gaussian spatial distributions. These space-dependent rate equations are solved numerically. From the numerical solutions, we obtain the dependences of pulse width, pulse repetition rate, single-pulse energy and peak power on pump power for the generated-green-laser pulses. The numerical solutions are consistent with the experimental results obtained from a diode-pumped passively Q-switched intracavity-frequency-doubling Nd:$GdVO_4$/KTP laser with Cr^{4+}:YAG saturable absorber.

2 Theoretical calculations

2.1 The longitudinal distribution of the photon density

We consider the laser depicted in Figure 1, in which Nd:$GdVO_4$ works as gain medium, KTP works as frequency-doubling crystal, and Cr^{4+}:YAG works as passive Q-switch. If the intracavity photon density is assumed to be a Gaussian spatial distribution during the entire formatting process of the LD-pumped passively Q-switched intracavity-frequency-doubling laser pulse, the intracavity photon density $\phi(r,t)$ for the TEM_{00} mode can be expressed as:

$$\phi(r,t) = \phi(0,t)\exp\left(-\frac{2r^2}{w_\mathrm{l}^2}\right), \tag{1}$$

where r is the radial coordinate; w_l is the average radius of the TEM_{00} mode, which is mainly determined by the geometry of the resonator; and $\phi(0,t)$ is the photon density in the laser axis. If the longitudinal distribution of the photon density along the cavity axis is considered, the photon densities $\phi_\mathrm{g}(r,t)$, $\phi_\mathrm{s}(r,t)$, and $\phi_\mathrm{k}(r,t)$ at three positions: Nd:$GdVO_4$ crystal, saturable absorber and KTP

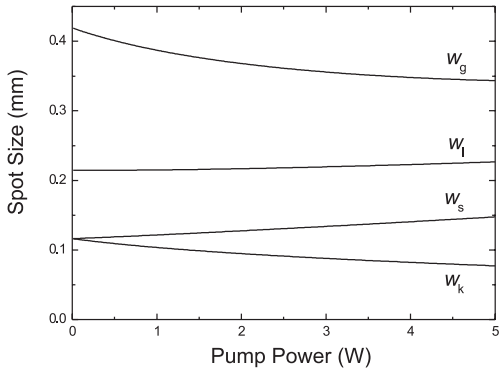

Fig. 2. Beam size versus pump power.

can be expressed as [15]:

$$\phi_\mathrm{g}(r,t) = \frac{w_\mathrm{l}^2}{w_\mathrm{g}^2}\phi(0,t)\exp\left(-\frac{2r^2}{w_\mathrm{g}^2}\right), \tag{2}$$

$$\phi_\mathrm{s}(r,t) = \frac{w_\mathrm{l}^2}{w_\mathrm{s}^2}\phi\,(0,t)\exp\left(-\frac{2r^2}{w_\mathrm{s}^2}\right), \tag{3}$$

$$\phi_\mathrm{k}(r,t) = \frac{w_\mathrm{l}^2}{w_\mathrm{k}^2}\phi\,(0,t)\exp\left(-\frac{2r^2}{w_\mathrm{k}^2}\right), \tag{4}$$

where w_g, w_s, and w_k are the radii of the TEM_{00} mode at the above-mentioned three positions, respectively.

In our experiment, however, the pump power is focused into the gain medium with a spot size of a few hundred microns, so the phase difference of it becomes uneven due to the un-uniformity of the temperature field distribution in the gain medium. The phase difference is distributed as a parabola profile and the gain medium has thermal lens effect, and the thermal focal length is [16]:

$$f_\mathrm{T} = \frac{2\pi K_\mathrm{c}}{\mathrm{d}n/\mathrm{d}T + \alpha_\mathrm{T} n_1}\frac{w_\mathrm{p}^2}{\xi P_\mathrm{in}\eta}, \tag{5}$$

where w_p is the radius of the pump light in the gain medium; η = 1-exp(-αl) is the absorptivity of the gain medium, in which α is the absorption coefficient and l is the length of the gain medium; P_in is the incident pump power; n_1 is the refractive index of the gain medium; and for our a-cut Nd:$GdVO_4$ crystal: $K_\mathrm{c} = 11.7\times 10^{-3}\,\mathrm{W\,mm^{-1}\,K^{-1}}$, $\mathrm{d}n/\mathrm{d}T = 4.7\times10^{-6}\,\mathrm{K^{-1}}$, $\xi = 0.24$, $\alpha_\mathrm{T} = 3.5\times10^{-6}\,\mathrm{K^{-1}}$.

For our experimental configuration shown in Figure 1, using the well-known ABCD matrix method [1] and considering the thermal lens effect of the gain medium, we have simulated w_g, w_s, w_k, and w_l as functions of incident pump power, and the results are shown in Figure 2.

2.2 Nonlinear loss due to harmonic conversion

For a Q-switched intracavity-frequency-doubling laser, the harmonic conversion is always considered as a nonlinear loss of the fundamental wave. Assuming that the fundamental wave (FW) is plane wave with Gaussian amplitude

profile:

$$E(\omega, r, z, t) = E(\omega, r)\cos(Kz - \omega t), \tag{6}$$

where ω is the angle frequency of the fundamental wave.

If the thermal effect and walking-off effect of KTP are neglected, the amplitudes for o and e light for KTP type-II phase matching are, respectively:

$$E_{\mathrm{o}}(\omega, r) = E_0^{\mathrm{o}} \exp\left(-\frac{r^2}{w_{\mathrm{k}}^2}\right), \tag{7}$$

$$E_{\mathrm{e}}(\omega, r) = E_0^{\mathrm{e}} \exp\left(-\frac{r^2}{w_{\mathrm{k}}^2}\right). \tag{8}$$

So the amplitude of second-harmonic wave (SHW) satisfies the following equation under the small-signal and near-field approximation [17]:

$$\frac{\mathrm{d}E(2\omega, r)}{\mathrm{d}z} = \mathrm{i}\frac{2\omega d_{\mathrm{eff}}}{n_{\mathrm{e}}^{2\omega} c} E_0^{\mathrm{o}} E_0^{\mathrm{e}} \exp\left(-\frac{2r^2}{w_{\mathrm{k}}^2}\right), \tag{9}$$

where d_{eff} is the effective nonlinear coefficient; c is the light velocity in vacuum; $n_{\mathrm{e}}^{2\omega}$ is the refraction index of SHW.

Integrating equation (9) along the z direction, yields:

$$E(2\omega, r) = \mathrm{i}\frac{2\omega d_{\mathrm{eff}} l_{\mathrm{k}}}{n_{\mathrm{e}}^{2\omega} c} E_0^{\mathrm{o}} E_0^{\mathrm{e}} \exp\left(-\frac{2r^2}{w_{\mathrm{k}}^2}\right), \tag{10}$$

where l_{k} is the length of KTP.

From the relationship between intensity and amplitude for light [17]:

$$I = \frac{1}{2} n c \varepsilon_0 \left|E^2\right|, \tag{11}$$

and the fundamental power [17]:

$$P^{\mathrm{i}} = \frac{\pi \omega_{\mathrm{k}}^2}{4} n c \varepsilon_0 \left|E_{\mathrm{i}}^2\right|, (\mathrm{i} = \mathrm{o}, \mathrm{e}) \tag{12}$$

we can obtain the SHW intensity at the exit of end face:

$$I(2\omega, r) = \frac{32\omega^2 d_{\mathrm{eff}}^2 l_{\mathrm{k}}^2}{c^3 \varepsilon_0 n_{\mathrm{e}}^{2\omega} n_{\mathrm{o}}^{\omega} n_{\mathrm{e}}^{\omega}} \frac{P_0^{\mathrm{o}} P_0^{\mathrm{e}}}{(\pi \omega_{\mathrm{k}}^2)^2} \exp\left(-\frac{4r^2}{w_{\mathrm{k}}^2}\right), \tag{13}$$

where ε_0 is the dielectric permeability of vacuum; n_{o}^{ω} and $n_{\mathrm{e}}^{\omega}$are fundamental-wave refractive indices of o and e light, respectively.

The FW intensity is:

$$\begin{aligned} I(\omega, r) &= I_{\mathrm{o}}(\omega, r) + I_{\mathrm{e}}(\omega, r) \\ &= \frac{1}{2} n_{\mathrm{o}}^{\omega} c \varepsilon_0 \left|E_{\mathrm{o}}(\omega, r)\right|^2 + \frac{1}{2} n_{\mathrm{e}}^{\omega} c \varepsilon_0 \left|E_{\mathrm{e}}(\omega, r)\right|^2 \\ &= \frac{2}{\pi \omega_{\mathrm{k}}^2} \exp\left(-\frac{2r^2}{w_{\mathrm{k}}^2}\right)(P_0^{\mathrm{o}} + P_0^{\mathrm{e}}). \end{aligned} \tag{14}$$

We assume:

$$P_0^{\mathrm{o}} = P_0^{\mathrm{e}} = (1/2)P(\omega, 0), \tag{15}$$

where $P(\omega, 0) = (1/2)A_{\mathrm{k}}\hbar\omega c\phi_{\mathrm{k}}(0, t)$ is the incident fundamental power in the axis of KTP, in which $A_{\mathrm{k}} = (1/2)\pi w_{\mathrm{k}}^2$ is the area of fundamental wave at the position of KTP, $\hbar\omega$ is the single photon energy of the fundamental wave, $\phi_{\mathrm{k}}(0, t)$ is the photon density in the laser axis at the position of KTP.

Table 1. Parameters of II-type phase-matching KTP crystal.

Parameters	Values
n_{o}^{ω}	1.83
n_{e}^{ω}	1.746
$n_{\mathrm{e}}^{2\omega}$	1.79
d_{eff}	7.2 pm/V
ε_0	$8.855 \times 10^{-12}\ \mathrm{C^2/N \cdot m^2}$

These data are provided by Coretech Crystal Company, Shandong University, China.

The nonlinear loss due to harmonic conversion can be obtained:

$$\begin{aligned} \delta_{\mathrm{N}} &= \frac{P(2\omega, r)}{P(\omega, r)} = \frac{I(2\omega, r)}{I(\omega, r)} \\ &= \frac{\omega^2 d_{\mathrm{eff}}^2}{c^3 \varepsilon_0 n_{\mathrm{e}}^{2\omega} n_{\mathrm{o}}^{\omega} n_{\mathrm{e}}^{\omega}} \hbar\omega c l_{\mathrm{k}}^2 \exp\left(-\frac{2r^2}{w_{\mathrm{k}}^2}\right)\phi_{\mathrm{k}}(0, t) \\ &= K_{\mathrm{N}} \hbar\omega c l_{\mathrm{k}}^2 \exp\left(-\frac{2r^2}{w_{\mathrm{k}}^2}\right)\phi_{\mathrm{k}}(0, t) \\ &= \delta_{\mathrm{k}}\phi_{\mathrm{k}}(r, t), \end{aligned} \tag{16}$$

where

$$K_{\mathrm{N}} = \frac{\omega^2 d_{\mathrm{eff}}^2}{c^3 \varepsilon_0 n_{\mathrm{e}}^{2\omega} n_{\mathrm{o}}^{\omega} n_{\mathrm{e}}^{\omega}}, \tag{17}$$

$$\delta_{\mathrm{k}} = K_{\mathrm{N}} \hbar\omega c l_{\mathrm{k}}^2. \tag{18}$$

The corresponding parameters for type-II phase-matching KTP crystal are presented in Table 1.

2.3 Rate equations

So for this laser, if neglecting the spontaneous radiation during the pulse formation, we can obtain the coupling rate equations [15]:

$$\begin{aligned} \int_0^{\infty} \frac{\mathrm{d}\phi(r, t)}{\mathrm{d}t} 2\pi r \mathrm{d}r = \int_0^{\infty} \frac{1}{t_{\mathrm{r}}} \{ & 2\sigma n(r, t) l \phi_{\mathrm{g}}(r, t) \\ & - 2\sigma_{\mathrm{g}} n_{\mathrm{s1}}(r, t) l_{\mathrm{s}} \phi_{\mathrm{s}}(r, t) \\ & - 2\sigma_{\mathrm{e}} \left[n_{\mathrm{s0}} - n_{\mathrm{s1}}(r, t)\right] l_{\mathrm{s}} \phi_{\mathrm{s}}(r, t) \\ & - \delta_{\mathrm{k}} \phi_{\mathrm{k}}^2(r, t) - L\phi(r, t) \} 2\pi r \mathrm{d}r, \end{aligned} \tag{19}$$

$$\frac{\mathrm{d}n(r, t)}{\mathrm{d}t} = R_{\mathrm{in}}(r) - \sigma c n(r, t)\phi_{\mathrm{g}}(r, t) - \frac{n(r, t)}{\tau}, \tag{20}$$

$$\frac{\mathrm{d}n_{\mathrm{s1}}(r, t)}{\mathrm{d}t} = \frac{n_{\mathrm{s0}} - n_{\mathrm{s1}}(r, t)}{\tau_{\mathrm{s}}} - \sigma_{\mathrm{g}} c n_{\mathrm{s1}}(r, t)\phi_{\mathrm{s}}(r, t), \tag{21}$$

where $n(r,t)$ is the average population-inversion density; $n_{s1}(r,t)$ and n_{s0} are the ground-state and total population densities of Cr^{4+}:YAG saturable absorber, respectively; σ and l are the stimulated-emission cross section and length of Nd:$GdVO_4$ gain medium, respectively; σ_g and σ_e are the ground-state and excited-state absorption cross sections of the saturable absorber, respectively; l_s is the length of the saturable absorber; t_r is the round-trip time of light in the resonator $\{t_r = [2n_1 l + 2n_2 l_s + 2n_3 l_k + 2(L_e - l - l_s - l_k)]/c\}$; n_1, n_2, and n_3 are the refractive indices of Nd:$GdVO_4$ gain medium, Cr^{4+}:YAG saturable absorber, and KTP crystal, respectively;l_k is the length of KTP; L_e is the cavity length; c is the velocity of light in vacuum; δ_k is given in equation (18); L is the intrinsic loss; τ is the stimulated-radiation lifetime of the gain medium;τ_s is the excited-state lifetime of the saturable absorber; $R_{in}(r) = P_{in}\exp(-2r^2/w_p^2)[1-\exp(-\alpha l)]/h\gamma_p \pi w_p^2 l$ is the pump rate, where $h\gamma_p$ is the single-photon energy of the pump light. The initial conditions of equations (20, 21) can be written as [15]:

$$n(r,0) = n(0,0)\exp\left(-\frac{2r^2}{w_p^2}\right), \tag{22}$$

$$n_{s1}(r,0) = n_{s0}, \tag{23}$$

where $n(0, 0)$ is the initial population-inversion density in the laser axis, i.e.,

$$n(0,0) = \frac{\ln\left(\frac{1}{T_0^2}\right) + L}{2\sigma l}\left(1 + \frac{w_g^2}{w_p^2}\right), \tag{24}$$

where $T_0 = \exp(-\sigma_g n_{s0} l_s)$ is the small-signal transmission of the saturable absorber.

Substituting equations (2, 3, 22, 23) into equations (20, 21) and integrating the results over time, we obtain:

$$\begin{aligned} n(r,t) = {} & \exp\left[-\sigma c\frac{w_l^2}{w_g^2}\exp\left(-\frac{2r^2}{w_g^2}\right)\int_0^t \phi(0,t)\mathrm{d}t - \frac{t}{\tau}\right] \\ & \times\left\{R_{in}(r)\int_0^t \exp\left[\sigma c\frac{w_l^2}{w_g^2}\exp\left(-\frac{2r^2}{w_g^2}\right)\right.\right. \\ & \left.\left.\times\int_0^t \phi(0,t)\mathrm{d}t + \frac{t}{\tau}\right]\mathrm{d}t + n(0,0)\exp\left(-\frac{2r^2}{w_p^2}\right)\right\}, \end{aligned} \tag{25}$$

$$\begin{aligned} n_{s1}(r,t) = {} & \exp\left[-\sigma_g c\frac{w_l^2}{w_s^2}\exp\left(-\frac{2r^2}{w_s^2}\right)\int_0^t \phi(0,t)\mathrm{d}t - \frac{t}{\tau_s}\right] \\ & \times\left\{\frac{n_{s0}}{\tau_s}\int_0^t \exp\left[\sigma_g c\frac{w_l^2}{w_s^2}\exp\left(-\frac{2r^2}{w_s^2}\right)\right.\right. \\ & \left.\left.\times\int_0^t \phi(0,t)\mathrm{d}t + \frac{t}{\tau_s}\right]\mathrm{d}t + n_{s0}\right\}. \end{aligned} \tag{26}$$

Table 2. Parameters of the theoretical calculation.

Parameters	Values	Parameters	Values
σ	$7.6\times10^{-19}\,\mathrm{cm}^2$	n_3	1.83
σ_g	$4.3\times10^{-18}\,\mathrm{cm}^2$	l_k	1.0 cm
σ_e	$8.2\times10^{-19}\,\mathrm{cm}^2$	l	0.5 cm
n_{s0}	$2.0\times10^{17}\,\mathrm{cm}^{-3}$	w_p	330 μm
τ	90 μs	L	0.08
τ_s	3.2 μs	α	5.49 cm^{-1}
n_1	2.19	ξ	0.85
n_2	1.81		

Data from references [10, 15].

Substituting equations (1–4) into equation (19), we obtain:

$$\begin{aligned} \frac{\mathrm{d}\phi(0,t)}{\mathrm{d}t} = {} & \frac{4\phi(0,t)}{w_l^2 t_r}\int_0^\infty \left\{2\sigma n(r,t) l\frac{w_l^2}{w_g^2}\exp\left(-\frac{2r^2}{w_g^2}\right)\right. \\ & -2\sigma_g n_{s1}(r,t) l_s\frac{w_l^2}{w_s^2}\exp\left(-\frac{2r^2}{w_s^2}\right) \\ & -2\sigma_e\left[n_{s0} - n_{s1}(r,t)\right] l_s\frac{w_l^2}{w_s^2}\exp\left(-\frac{2r^2}{w_s^2}\right) \\ & -\delta_k\phi(0,t)\frac{w_l^4}{w_k^4}\exp\left(-\frac{4r^2}{w_k^2}\right) \\ & \left.-L\exp\left(-\frac{2r^2}{w_l^2}\right)\right\} r\mathrm{d}r, \end{aligned} \tag{27}$$

where $n(r,t)$ and $n_{s1}(r,t)$ are given in equations (25, 26). Equation (27) is the basic differential equation describing $\phi(0,t)$ as a function of t. From the relation between $\phi_k^2(0,t)$ and t, we can obtain the pulse width (FWHM) W and the pulse repetition rate F of the generated-green-light pulses. The pulse peak power P and the single-pulse energy E can be expressed as:

$$P = \frac{1}{2}\xi K_N A_k l_k^2 (\hbar\omega c)^2 \phi_{km}^2, \tag{28}$$

$$E = \frac{1}{2}\xi K_N A_k l_k^2 (\hbar\omega c)^2 \phi_{int}, \tag{29}$$

where ξ is the fraction that coupled out the resonator; K_N is given in equation (17); $A_k = (1/2)\pi w_k^2$ is the area of fundamental wave at the position of KTP; ϕ_{km} is the maximum value of $\phi_k(0,t)$; ϕ_{int} is the integral of $\phi_k^2(0,t)$ over t from the beginning time t_1 to ending time t_2 of the single pulse.

The corresponding parameters values of the theoretical calculation are shown in Table 2, in which we mainly adjust the value of L to fit the experimental data. The small-signal transmissions of two Cr^{4+}:YAG saturable absorbers are $T_0 = 0.87$ and $T_0 = 0.95$, respectively. The dotted line in Figure 3 shows the theoretical pulse shape at $T_0 = 0.87$ and a pump power of 3.4 W. The solid lines in Figures 4–7 are the theoretical calculation curves for pulse width W, pulse repetition rate F, single-pulse energy E, and peak power P versus pump power, respectively.

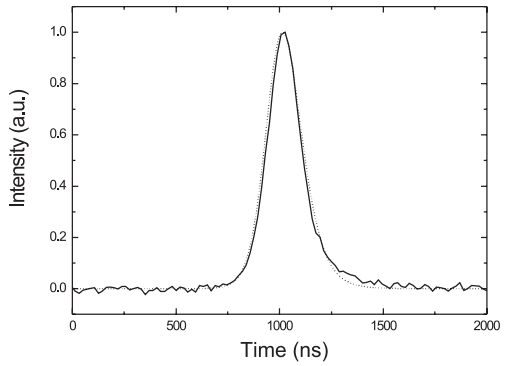

Fig. 3. Temporal profile of single pulse with Cr^{4+}:YAG $T_0 = 0.87$. Solid line, oscilloscope trace; dotted line, calculated result.

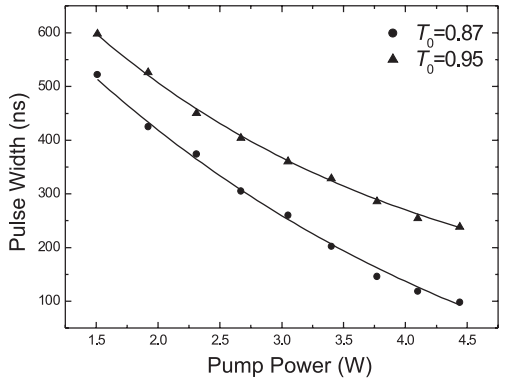

Fig. 4. Pulse width versus pump power. Solid lines, theorical results; scattered dots, experimental results.

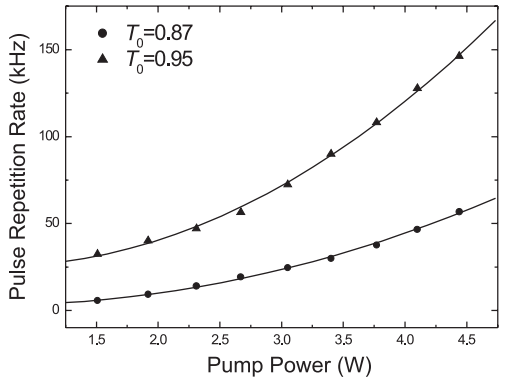

Fig. 5. Pulse repetition rate versus pump power. Solid lines, theoretical results; scattered dots, experimental results.

3 Experimental setup and results

The experimental setup is shown in Figure 1. The pump source is a fiber-coupled laser-diode (made by Semiconductor Institute, Chinese Academic, maximum output power 5 W) which works at the maximum absorption wavelength (808 nm) of the Nd:$GdVO_4$ crystal. The mirror M_1 with 150-mm curvature radius is high antireflection coated at 808 nm and high reflection coated at 1064 nm and 532 nm. The Nd:$GdVO_4$ crystal doped with

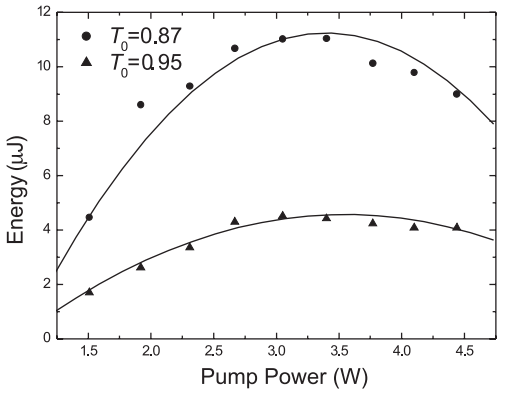

Fig. 6. Single-pulse energy versus pump power. Solid lines, theoretical results; scattered dots, experimental results.

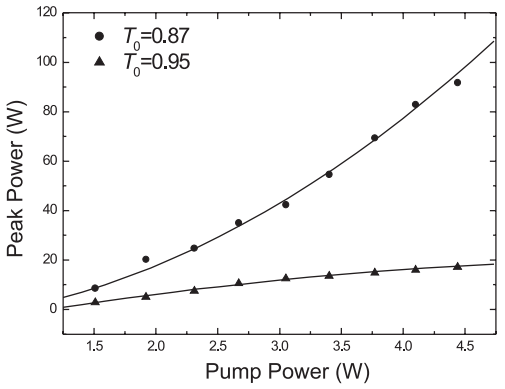

Fig. 7. Pulse peak power versus pump power. Solid lines, theoretical results; scattered dots, experimental results.

1.0 at.% Nd^{3+} ions is 4×4×5 mm^3 and its absorption coefficient at 808 nm is 5.49 cm^{-1}. Its first surface is antireflection coated at 808 nm and the other surface is high antireflection coated at 1064 nm. It is near M_1. The mirror M_3 with 100-mm curvature radius is also used as the output mirror of the generated green light, and it has a reflectivity of 99.6% at 1064 nm and a transmission of 85% at 532 nm. The KTP crystal cut for type-II phase matching (made by Coretech Crystal Company, Shandong University, China) is 3×3×10 mm^3 and both of its surfaces are antireflection coated at 1064 nm and 532 nm. The temperatures of the Nd:$GdVO_4$ crystal and the KTP crystal are controlled at 20 °C and 22 °C by means of a temperature controller, respectively. M_2 is a plane mirror and its surface is high reflection coated at 1064 nm and 532 nm. The KTP crystal is near M_2. The distance between M_1 and M_3 is about 22 cm, the distance between saturable absorber and M_3 is about 8 cm, and the distance between M_2 and M_3 is about 8 cm. The filter is used for separating 532-nm green laser from the remainder 1064-nm fundamental wave leaking out from the resonator. A LPE-1B power meter (Institute of Physics, Chinese Academy of Science) is used to measure the generated-green-laser power and a TED620B digital oscilloscope (Tektronix Inc., USA) is used to measure the generated-green-laser pulse width and pulse repetition rate.

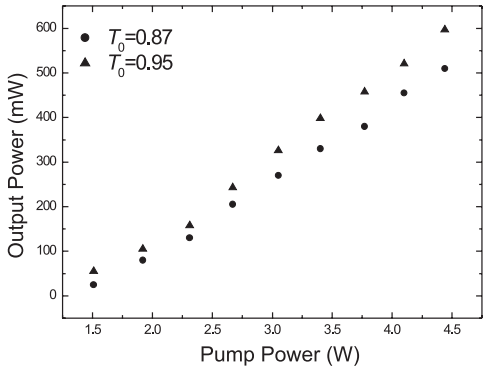

Fig. 8. Average output power versus pump power.

Figure 8 shows the average output power P_a of the generated-green-laser pulses versus pump power. A single-pulse temporal profile of an oscilloscope trace at $T_0 = 0.87$ and a pump power of 3.4 W is shown by the solid line in Figure 3. The dependences of pulse width W and pulse repetition rate F of the generated-green-laser pulses on pump power are shown by scattered dots in Figures 4 and 5. Using the equations $E = P_a/F$ and $P = E/W$, we obtain the single-pulse energy E and the peak power P, which are shown by scattered dots in Figures 6 and 7. From Figures 3–7, we can see that the experimental results are in agreement with the theoretical calculations.

However, it should be pointed out that the influences of the multi-longitude-mode coupling have been neglected in our theoretical calculation. In fact, the longitudinal-mode coupling and sum-frequency generation may lead to intensity fluctuations of the output green laser. Under relatively high pump power, the modulated Q-switched pulses have been observed in our experiment. For a-cut Nd:$GdVO_4$ crystal, the π-polarization emission cross section is much larger than that of the σ-polarization, which will result in π-polarization mode oscillation in cw lasers whatever the polarization direction of pump light is. However, for the intracavity-frequency-doubling Nd:$GdVO_4$/KTP green laser, the KTP crystal acts as birefringent filter due to its anisotropy. The σ-polarized mode can exist in the resonator, especially under high pump power. There are two effects relevant to this dynamical process [18]: mode coupling related to the presence of standing waves in the gain medium on the microsecond timescale of the cavity relaxation oscillations, and couplings associated with sum generations on the nanosecond timescale of the cavity lifetime. We believe that the modulation phenomenon results from the frequency beat of the two polarized-mode eigenstates and the modulation process can be theoretically simulated with the multi-longitude-mode rate equations [19].

4 Conclusions

We have assumed the intracavity photon density to be Gaussian spatial distributions and the nonlinear loss due to SHG is also given under Gaussian spatial distributions in the rate equations of a diode-pumped passively Q-switched intracavity-frequency-doubling Nd:$GdVO_4$/KTP laser with Cr^{4+}:YAG saturable absorber. These space-dependent rate equations are solved numerically. From the numerical solutions, we obtain the dependences of pulse width, pulse repetition rate, single-pulse energy and peak power on pump power for the generated-green-laser pulses. The theoretical calculations of the numerical solutions agree with the experimental results obtained from a diode-pumped passively Q-switched intracavity-frequency-doubling Nd:$GdVO_4$/KTP laser with Cr^{4+}:YAG saturable absorber.

This work is partially supported by the Science and Technology Development Program of Shandong Province and the Research Fund for the Doctoral Program of Higher Education.

References

1. A.E. Siegman, *Lasers* (University Science Books, Mill valley, 1986)
2. W. Koechner, *Solid-State Laser Engineering* (Springer, Berlin, 1996)
3. T. Taira, T. Kobayashi, Appl. Opt. **34**, 4298 (1995)
4. A. Agnesi, S. Dell'Acqua, E. Piccinini, G. Reali, G. Piccinno, IEEE J. Quantum Electron. **34**, 1480 (1998)
5. A.I. Zagumennyi, V.G. Ostroumov, I.A. Shcherbakov, T. Jensen, J.P. Meyn, G. Huber, Sov. J. Quant. Electron. **22**, 1071 (1992)
6. T. Jensen, V.G. Ostroumov, J.P. Meyn, G. Huber, A.I. Zagumennyi, I.A. Shcherbakov, Appl. Phys. B **58**, 373 (1994)
7. J. Liu, J. Yang, J. He, Opt. Commun. **219**, 317 (2003)
8. P.A. Studenikin, A.I. Zagumennyi, Y.D. Zavartsev, P.A. Popov, I.A. Shcherbakov, Quant. Electron. **25**, 1162 (1995)
9. C. Li, J. Song, D. Shen, N.S. Kim, J. Lu, K. Ueda, Appl. Phys. B **70**, 471 (2000)
10. J. Liu, C. Wang, C. Du, L. Zhu, H. Zhang, X. Meng, J. Wang, Z. Shao, M. Jiang, Opt. Commun. **188**, 155 (2001)
11. J. Liu, B. Ozygus, S. Yang, J. erhard, U. Seelig, A. Ding, H. Weber, J. Opt. Soc. Am. B **20**, 652 (2003)
12. J. Liu, C. Du, Z. Wang, L. Zhu, H. Zhang, X. Meng, J. Wang, Z. Shao, M. Jiang, Opt. Laser Technol. **33**, 177 (2001)
13. J. Liu, C. Wang, C.Q. Wang, X. Meng, H. Zhang, L. Zhu, J. Wang, Z. Shao, M. Jiang, Appl. Phys. B **72**, 171 (2001)
14. J. Liu, J. Yang, J. He, Opt. Laser Technol. **36**, 31 (2004)
15. G. Li, S. Zhao, H. Zhao, K. Yang, S. Ding, Opt. Commun. **234**, 321 (2004)
16. J. Zheng, S. Zhao, Q. Wang, X. Zhang, L. Chen, Acta Photon. Sin. **30**, 724 (2001) (in Chinese)
17. J. Zheng, S. Zhao, Q. Wang, X. Zhang, L. Chen, Opt. Commun. **199**, 207 (2001)
18. D.W. Anthon, D.L. Sipes, T.J. Pier, M.R. Ressl, IEEE J. Quantum Electron. **28**, 1148 (1992)
19. J. Zheng, S. Zhao, L. Chen, Chin. J. Lasers **B11**, 241 (2002)